JGR Oceans

RESEARCH ARTICLE
10.1029/2020JC016849

Variations of the Kuroshio in the Luzon Strait Revealed by EOF Analysis of Repeated XBT Data and Sea-Level Anomalies

Yu Long[1], Xiao-Hua Zhu[1,2,3], Xinyu Guo[1,4], Fei Ji[1], and Zhiyuan Li[5]

[1]State Key Laboratory of Satellite Ocean Environment Dynamics, Second Institute of Oceanography, Ministry of Natural Resources, Hangzhou, China, [2]Southern Marine Science and Engineering Guangdong Laboratory, Zhuhai, China, [3]School of Oceanography, Shanghai Jiao Tong University, Shanghai, China, [4]Center for Marine Environmental Study, Ehime University, Matsuyama, Japan, [5]Key Laboratory for Technology in Rural Water Management of Zhejiang, Zhejiang University of Water Resources and Electric Power, Hangzhou, China

Key Points:

- Variations of the Kuroshio in the Luzon Strait (LS) were examined by analyzing sectional water temperature and sea-level anomaly data
- Kuroshio-South China Sea water exchange contributes to the opposite seasonal variation in volume transport from east of Luzon to the LS
- Westward propagated eddies along 21°–24°N and variations from the North Equatorial Current bifurcation impact the Kuroshio in the LS

Supporting Information:

Supporting Information may be found in the online version of this article.

Correspondence to:

X.-H. Zhu,
xhzhu@sio.org.cn

Citation:

Long, Y., Zhu, X.-H., Guo, X., Ji, F., & Li, Z. (2021). Variations of the Kuroshio in the Luzon Strait revealed by EOF analysis of repeated XBT data and sea-level anomalies. *Journal of Geophysical Research: Oceans*, *126*, e2020JC016849. https://doi.org/10.1029/2020JC016849

Received 6 OCT 2020
Accepted 10 JUN 2021

Abstract The Kuroshio in the Luzon Strait (KLS) has long been a focus of research for its complex ocean dynamics; however, it is poorly understood owing to a lack of long-term *in situ* observations. Empirical orthogonal function (EOF) analyses were applied to quarterly expendable bathythermograph data (XBT, with a spatial resolution of 10–20 km in the Kuroshio region and 33 km in the other regions) and sea-level anomaly (SLA) data, to examine the variations of the KLS. The first EOF modes of water temperature and SLA represent seasonal variations. The volume transport of the KLS referring to a 700 m depth reaches its maximum in warm months (19.4 Sv, July–September) and its minimum in cold months (17 Sv, January–March). This variation is similar to that east of Taiwan but is opposite to that east of Luzon, although the Luzon Strait is only 2° distant from the area east of Luzon. The outflow (1.3 Sv) from the South China Sea (SCS) to the Kuroshio in the warm months and the Kuroshio intrusion into the SCS in the cold months are responsible for this seasonal contrast. The second EOF modes of water temperature and SLA are related to the latitudinal movement of the Kuroshio recirculation on a time scale of 2–24 months. Lag correlation and wavelet analysis demonstrate that this mode is triggered by the westward-propagating SLA along 21°–24°N and is affected by the downstream propagation of low-frequency variation (mostly annual to biennial) from the North Equatorial Current bifurcation area.

Plain Language Summary Variations of the Kuroshio in the Luzon Strait (KLS) from 1999 to 2010 were examined by using sea-level anomaly (SLA) data and long-term repeated water temperature data observed by expendable bathythermography (XBT, cast by automatic launchers equipped on commercial ships). The decomposition (empirical orthogonal function, EOF) analysis of the two datasets shows that the most dominant components represent seasonal variations. The volume transport of the KLS reaches a maximum in warm months (July–September) and a minimum in cold months (January–March), which is similar to the seasonal variation of the Kuroshio east of Taiwan but is opposite to that east of Luzon. The Kuroshio-South China Sea (SCS) water exchange is the main cause of the reversed seasonal variation in the Kuroshio transport between the area east of Luzon and the Luzon Strait. The second dominant components represent the latitudinal movement of the Kuroshio recirculation and result from the westward-propagating SLA along 21°–24°N and the downstream propagation of low-frequency variation from the area where the North Equatorial Current bifurcates into the Kuroshio and Mindanao Current. This work has implications for the Kuroshio-SCS water exchange and Kuroshio-eddy interactions from east of Luzon to the east of Taiwan.

1. Introduction

The Kuroshio transports tremendous amounts of heat, salt, and nutrients poleward and has a large impact on adjacent marginal seas (Atkinson, 2010). Among these, the South China Sea (SCS) has been the focus of oceanographers, owing to its frequent water exchange with the Kuroshio (e.g., Farris & Wimbush, 1996; Hu et al., 2000; Liu et al., 2008; Nan et al., 2015; Shaw, 1991; Wu & Hsin, 2012). As the Luzon Strait (LS) is the only passage connecting the Kuroshio and the SCS, the LS has received much attention.

Previous studies conducted in the LS have involved a wide range of topics, including the Kuroshio-SCS water exchange (Qu et al., 2000), Kuroshio-eddy interactions (Lien et al., 2014; Z. Sun et al., 2020; Zheng et al., 2011), propagated and nonpropagated sea-level anomalies (Nan, Xue, et al., 2011; D. Yuan et al., 2006), and variations in the Kuroshio axis (Nan, He, et al., 2011). Generally, these topics are interconnected. For example, the eddy impinging on the Kuroshio may alter its axis, from a leaping path that flows directly northward across the LS to a penetrating path that loops toward the SCS (D. Yuan et al., 2019). This Kuroshio-eddy interaction may induce an eddy-shedding event, which offers a route for water exchange between the Kuroshio and the SCS (Z. Zhang et al., 2017) and impacts upper layer circulation in the SCS (Lin et al., 2016; Wang et al., 2019, 2020; Xu and Oey, 2014, 2015; Z. Zhang et al., 2013).

Local ocean dynamics are highly variable both spatially and temporally. For example, R. Sun et al. (2016) reported that the Kuroshio in the LS bifurcates into two branches. The western branch varies on a seasonal basis, and the eastern branch shows intraseasonal and interannual variability associated with mesoscale eddies. Y. Yuan et al. (2014) demonstrated that the winter intrusion in 2008 could be attributed to monsoon winds, and the summer intrusion in 2009 was affected by the El Niño-Southern Oscillation (ENSO). Hence, one- or two-year mooring observations at one or several stations (Andres et al., 2017; Liang et al., 2008; Lien et al., 2014; Y. Yuan et al., 2014; Z. Zhang et al., 2015) or snapshot ship-based surveys (Li et al., 1998; Jan et al., 2015) showed different results and were difficult to compare.

Generally, the Kuroshio in the LS varies at different time scales owing to variations in the local wind, volume transport of the Kuroshio or its branches, subtropical gyre, or Kuroshio-eddy interactions. Nan et al. (2015) demonstrated that the Kuroshio volume transport in the LS is large in summer but small in winter. For the Kuroshio east of Luzon, Yaremchuk and Qu (2004) demonstrated that the annual variation in its volume transport at 18.5°N reached a maximum of ~32 Sv in March–April and a minimum of ~23 Sv in October–November (Figure 14 in their paper). On the other hand, Lien et al. (2014) reported that the volume transport of the Kuroshio east of Luzon exhibited a positive anomaly in winter and a negative anomaly in summer and autumn, based on their analysis of mooring and altimetry data. For the Kuroshio east of Taiwan, Gilson and Roemmich (2002) demonstrated that its volume transport reaches a maximum in July (25.6 Sv) and a minimum in April (17.2 Sv). These results show that the Kuroshio east of Luzon and east of Taiwan exhibit different seasonal variations in their volume transport. However, the cause of this difference is not clear.

Some studies have used sea-level anomaly (SLA) data to show long-term variations in the local eddy field (Yan et al., 2016) and Kuroshio intrusion (Nan, He, et al., 2011). Although SLA data have advantages in terms of spatial coverage and temporal resolution, they do not provide a vertical structure and have limitations in terms of understanding the detailed dynamics. Hence, long-term repeated hydrographic observations are a good complement to SLA data. Unfortunately, there is no repeated conductivity-temperature-depth (CTD) section in the LS. As a secondary choice, long-term repeated expendable bathythermograph (XBT) observations conducted by commercial ships can be a good alternative for revealing the variations of the Kuroshio in the LS.

Empirical orthogonal function (EOF) analysis is widely used to study the variations of the Kuroshio in the LS and east of Taiwan. For example, Yan et al. (2016) applied EOF analysis within the region 121°–125°E and 21°–25°N to understand how mesoscale eddies impact Kuroshio volume transport east of Taiwan. Sheu et al. (2010) examined eddy propagation by applying EOF analysis to 10-year model output within the region 121°–128°E and 15°–28°N. Applying EOF analysis to the PCM1 mooring data set, D. Zhang et al. (2000) demonstrated that ~60% of the total subinertial variances in velocity and temperature in the Kuroshio east of Taiwan were associated with volume transport and current axis variation. This study applied EOF analysis to SLA data spanning the LS region and water temperature data at the PX44 section collected by the Scripps High Resolution XBT program from 1999 to 2010 to extract the dominant variations of the Kuroshio in the LS, at the sea surface and at depth. Moreover, the flow structures under the modulation of the EOF modes are shown by calculating the corresponding mean geostrophic velocity normal to the section.

In the next section, we provide a brief description of the data used in this study. Section 3 presents our results, and Sections 4 and 5 present our discussion and summary, respectively.

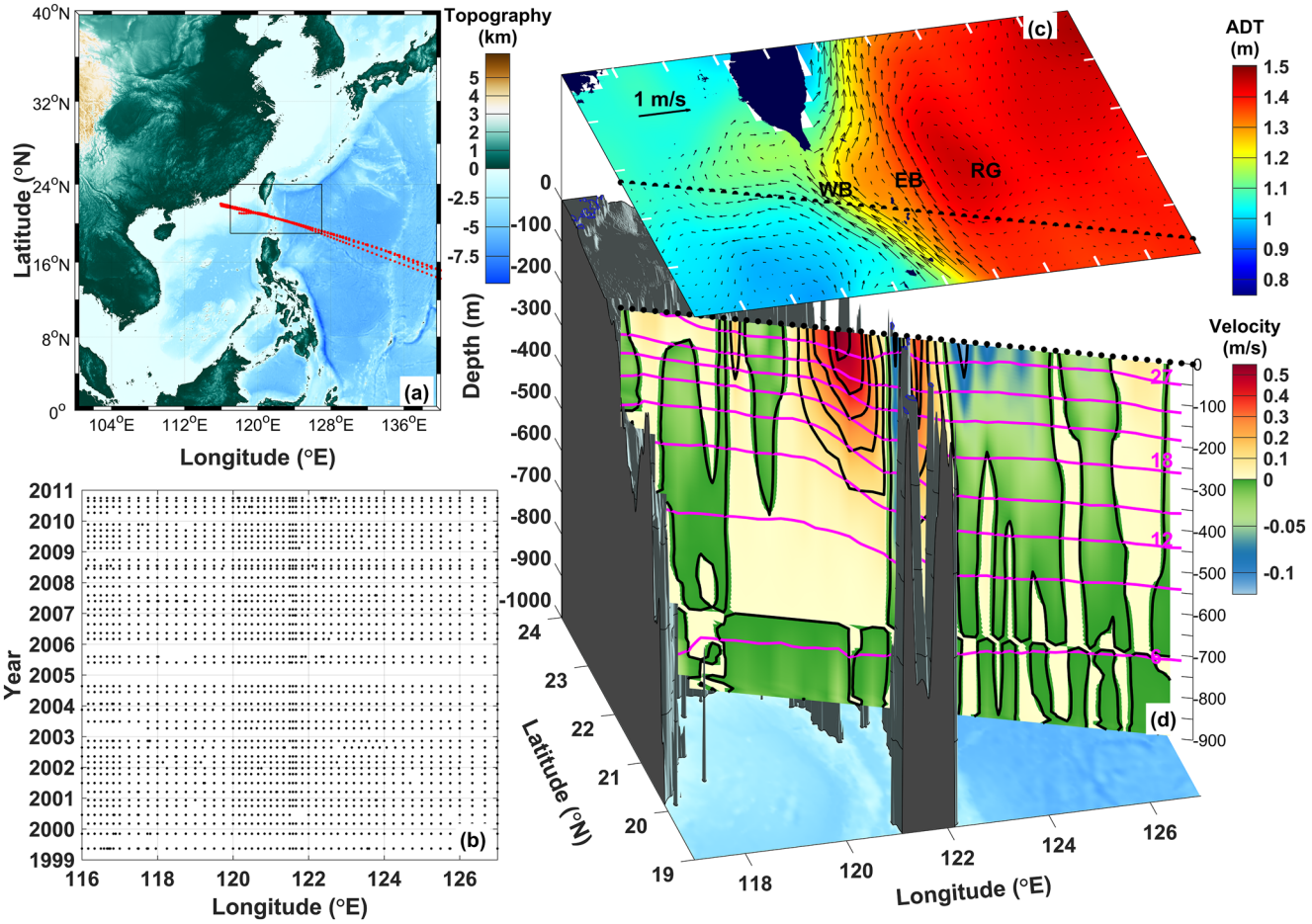

Figure 1. (a) Map and location of the expendable bathythermography (XBT) casts (red dots); the black rectangle indicates the study area shown in (c). (b) XBT casts as a function of time and longitude; (c) mean absolute dynamic topography (ADT, color shading) and surface geostrophic velocity (black arrows), WB, EB and RG represent the west branch and the east branch of the Kuroshio and Kuroshio recirculation gyre, respectively; and (d) mean geostrophic velocity normal to the section and water temperature (purple lines) at the PX44 section. The black dots in (c and d) denote the data points used to calculate geostrophic velocity.

2. Data

The high-resolution XBT network supported by commercial ships, which cruise at a typical speed of 21 knots and cover the LS within 1–2 days (Figure 1a), offers us a quarterly eddy-resolving view of the upper ocean thermal structure (Sprintall & Roemmich, 1999). Gilson and Roemmich (2002) analyzed data collected along the PX44 line (PX-44HK from California to Hong Kong and PX-44Ka from California to Kao-Hsiung) from 1993 to 2001 and suggested that the mean geostrophic transport of the Kuroshio in the upper 800 m was 22 ± 1.5 Sv, and its variation is affected by the impingement of westward-propagating mesoscale eddies. Since then, XBT observations at the PX-44HK line continued until 2010, and there have been 43 cruises (Figure 1b) that provide us with a quarterly sampling, high-spatial resolution (10–20 km in the Kuroshio and 33 km in the other region) and long duration (1999–2010) data set, allowing an analysis of long-term variations in the Kuroshio in the LS.

Salinity data were obtained from the "Grid Point Value of the Monthly Objective Analysis using the Argo data" data set (MOAA-GPV, Hosoda et al., 2008), which has a horizontal resolution of 1°. For the period before February 2001 (6 cruises in all) when there were no salinity data to match the XBT data, we used the monthly mean salinity in the same month of XBT data. The error caused by uncertainties in salinity is less than 2 cm/s for the velocity and less than 0.5 Sv for the volume transport (additional details on the error estimation are provided in the supplemental information).

The geostrophic velocity was calculated along the section where XBT data (117.5°–125.0°E) and MOAA-GPV data (118.5°–125.0°E) overlap (i.e., 118.5°–125.0°E). When computing the geostrophic velocity, we resampled the original temperature data at 0.2° intervals (the water temperature was first horizontally interpolated with a 0.05° interval, then filtered with a cutoff of 0.2°, and finally interpolated with an interval of 0.2°) to remove abrupt variations that may have resulted from small-scale dynamics and set the no-motion level at 700 m depth. Because the Kuroshio was confined to the upper 700 m in the LS and east of Taiwan (Andres et al., 2017; Gilson & Roemmich, 2002; Jan et al., 2015), the calculated geostrophic velocity referring to a depth of 700 m can capture most variations in the Kuroshio.

We also used SLA and absolute dynamic topography (ADT) data to obtain sea-surface information. These data were obtained from AVISO (Archiving, Validation, and Interpretation of Satellite Oceanographic data), with a spatial resolution of 1/4° × 1/4°, covering the period from 1993 to 2017. To determine the surface velocity field in the LS, we collected trajectory data of the Argos drifter (1979–2019) at a depth of 15 m from the World Ocean Circulation Experiment—Surface Velocity Programme (WOCE-SVP). In addition, temperature and salinity data from Argo floats were used to examine the variation in water properties from east of Luzon to the east of Taiwan.

EOF analysis was conducted within the area 115°–127°E and 15°–25°N, both for XBT and SLA data at locations deeper than 200 m. Because the EOF results depend on the choice of spatial and temporal coverage of the data, a sensitivity test was also performed to ensure consistency between the EOF results of daily SLA data and quarterly XBT data. By definition, the input data (**X**) have the following form:

$$\mathbf{X} = \left(X_{ij}\right)_{m\times n} = \begin{pmatrix} X_{11} & X_{12} & \cdots & X_{1n} \\ X_{21} & X_{21} & \cdots & X_{2n} \\ \vdots & \vdots & & \vdots \\ X_{m1} & X_{m2} & \cdots & X_{mn} \end{pmatrix},$$

where n is the number of data in space and m denotes the number of data in time.

The EOF result has the form of

$$X_{ij} = \sum_{k=1}^{m} P_{ik}T_{kj}, i = 1,2,\cdots,m; j = 1,2,\cdots,n$$

where k is the number of modes, P_{ik} is the orthogonal spatial pattern and T_{kj} are the corresponding principal components whose magnitudes were normalized to 1.

Supposing there is a full data set (data A) with a sufficiently short temporal interval and another data set (data B) with a long temporal interval, the question between daily SLA data and quarterly XBT data becomes whether the EOF modes derived from data A can be recognized by the EOF results of data B. For this purpose, we set data A as daily SLA and prepared data B by resampling daily SLA using the time of quarterly XBT.

We present the spatial pattern and principal component of the first (Figures 2a–2c) and second (Figures 2d–2f) EOF modes of SLA from daily SLA and quarterly resampled SLA corresponding to 43 XBT cruises. The spatial patterns show consistency in the positive area west of Luzon in the first EOF mode (Figures 2a and 2b) and in the negative area east of Taiwan in the second EOF mode (Figures 2d and 2e). In the area where the variation is small, although the corresponding spatial patterns do not match well, it does not affect the conclusion of this study. Additionally, the corresponding principal components (Figures 2c and 2f) show similar variations, confirming that these two modes can be recognized by the sparse sample at the time of the XBT cruise.

The potential spicity (π, a function of temperature, salinity and pressure, R. X. Huang et al., 2018) was used to distinguish water masses and calculate their mixing ratio between the end members at the same potential density (σ). σ-π space has advantages over traditional T-S space on account of its orthogonal nature (R. X. Huang et al., 2018).

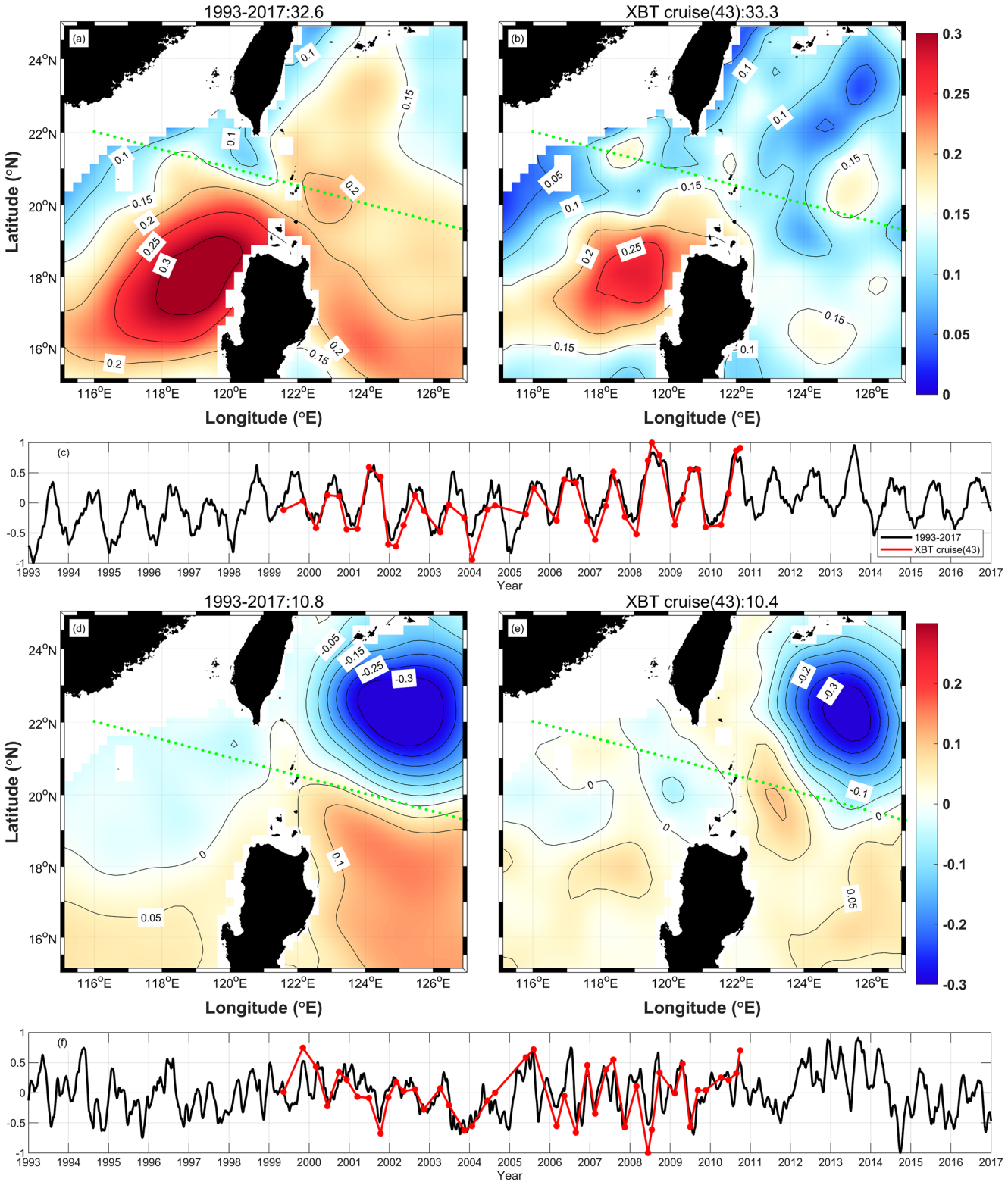

Figure 2. The comparison of the first (a–c) and second (d–f) SLA-EOF results using the entire datasets (black line) and SLA data during the expendable bathythermography (XBT) casts (red line). (a, b, d, and e) are the spatial patterns (the numbers at the end of the title are its explanation, and green dots represent the PX44 line), and (c and f) are the corresponding principal components.

3. Results

The surface geostrophic velocities demonstrate that the Kuroshio in the LS zonally expands from 119.0°E to 123.0°E (Figure 1c). The geostrophic current given by XBT data shows two branches: a west branch (118.8°–121.8°E) with large volume transport (16.1 ± 6.7 Sv, mean ± standard deviation) and an east branch (122.0°–123.0°E) with small volume transport (6.1 ± 6.2 Sv, Figure 1d). The negative (southward) velocity east of 123.0°E is a part of the local recirculation gyre (123°–124.6°E, Figures 1c and 1d) and has a volume transport of −2.6 ± 9.1 Sv. In addition, the negative velocity between the two Kuroshio branches is the island wake of the Kuroshio, and its maximum velocity exceeds 0.1 m/s. The volume transport integrated over the entire Kuroshio region (118.8°–124.6°E) is 18.7 ± 7.2 Sv, in which the large standard deviation of 7.2 Sv suggests that the Kuroshio in the LS is highly variable.

The EOF analysis decomposes the standing variations in both the SLA data and water temperature into orthogonal modes. More than 40% of the total variance in the SLA (33.2% and 9.5%, respectively) and sectional water temperature (27.5% and 14.6%, respectively) can be explained by the first two EOF modes.

The first EOF modes of water temperature and SLA represent seasonal variations (Figure 3). The large positive value (3°C) in the spatial pattern of water temperature (Figure 3a) in the surface layer corresponds to seasonal heating and cooling. In the subsurface layer, the spatial pattern is horizontally diverse, with positive values east of 121.0°E and negative values at a depth of ∼250 m between 120.0°E and 121.0°E. Further to the west, the spatial pattern is vertically reversed, with positive values in the upper 600 m and negative values in the deeper layer. The spatial pattern of ADT (Figure 3b) exhibits an in-phase variation with a maximum value west of Luzon where the Luzon cold eddy was reported (Z. Huang et al., 2019). The corresponding principal component consists of seasonal variation and weak interannual variation (Figure 3c). Both the climatological daily mean of the SLA principal component and the climatological monthly mean of the water temperature principal component (Figure 3d) indicate peaks in warm months (July, August, and September) and troughs in cold months (January, February, and March), confirming the nature of seasonal variation.

To understand the first EOF mode, we prepared composite maps. The mean water temperature and geostrophic velocity for the period when the principal component of the first EOF mode of water temperature was larger (smaller) than its positive (negative) standard deviation was calculated. The mean ADT for the period when the principal component of the first EOF mode of the SLA was larger (smaller) than its positive (negative) standard deviation was calculated. As shown in Figure 3d, the former occurs in warm months, while the latter occurs in cold months. The isotherms in the Kuroshio region are steeper in warm months (Figure 4a) than in cold months (Figure 4d), indicating that the Kuroshio is stronger in warm months than in cold months. The SLA shows that the Kuroshio in warm months flows northward and leaps over the LS, along with a strong Kuroshio recirculation east of the LS (Figure 4b). In cold months (Figure 4e), part of the Kuroshio penetrates into the SCS, the LS cold eddies become apparent and the local Kuroshio recirculation gyre becomes weaker, in accordance with our general knowledge on the seasonal variation in local circulation.

The composite geostrophic velocity shows that the currents normal to the section, both northward and southward, are stronger and narrower in warm months than in cold months (Figures 4c and 4f). Consequently, the two branches and local recirculation gyre exhibit a larger volume transport through the section in warm months than in cold months (Table 1). In addition, the net volume transport over the entire Kuroshio region also attains its maximum in warm months and minimum in cold months. The large standard deviation in the volume transport indicates that the currents in the LS are highly variable. The flow width exhibits an opposite variation compared with the volume transport; that is, when the volume transport is large, the flow width is small, and vice versa.

The second EOF mode of water temperature (Figure 5a) represents a longitudinally reversed variation. Its subsurface maximum is located at a depth of ∼100 m, with a maximum of −2°C on the SCS side and a maximum of 4°C on the Pacific side. The second EOF mode of the SLA (Figure 5b) presents a large magnitude on the Pacific side that has a latitudinal seesaw structure. The location of the PX44 line allows the XBT to observe a negative phase on the SCS side and a positive phase on the Pacific side.

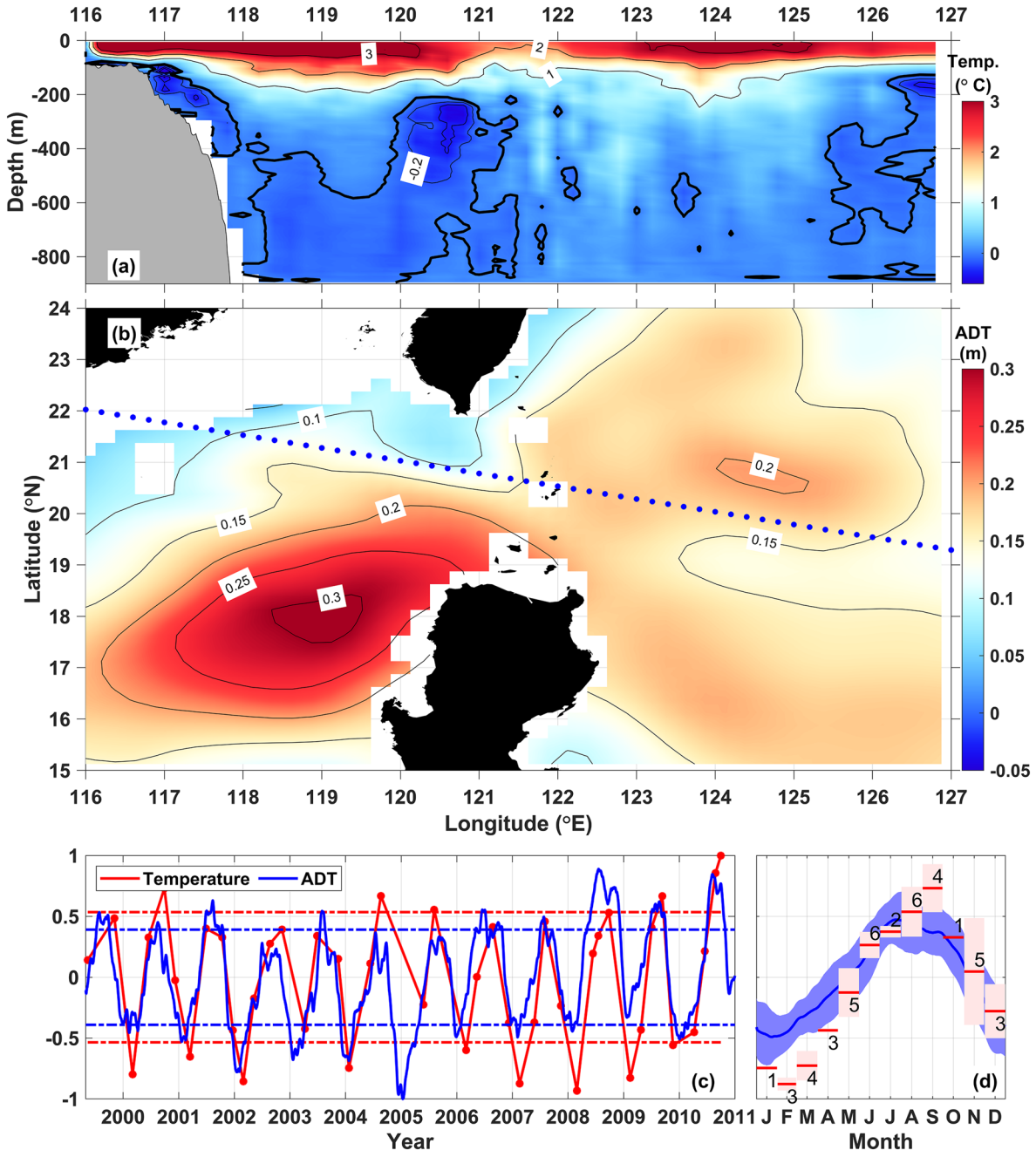

Figure 3. (a) Spatial pattern of the first EOF mode of water temperature (contour interval: 0.2°C for negative values and 1°C for positive values; the thick black line represents 0°C). (b) Spatial pattern of the first empirical orthogonal function (EOF) mode of SLA (contour interval: 0.05 m). Blue dots represent the PX44 line. (c) The principal components of the first modes of water temperature (red line) and sea-level anomaly (SLA, blue line). The dashed line represents positive and negative standard deviations. (d) The seasonal cycle of two principal components in (c). The thick blue line (shading) represents the daily mean (standard deviation) of the principal component of the first EOF mode of SLA. The thick red line (shading) represents the monthly mean (standard deviation) of the principal component of the first EOF mode of water temperature. The values around the thick red lines are the data numbers used for calculating the mean and standard deviation.

We also prepared a composite map of water temperature and ADT for their second EOF mode (Figure 6). The isotherms exhibit a larger slope in the Kuroshio region during the period when the principal component of the second EOF mode of water temperature is larger than its positive standard deviation (Figure 6a) compared with the period when the principal component of the second EOF mode of water temperature is smaller than its negative standard deviation (Figure 6d). When the principal component of the second EOF

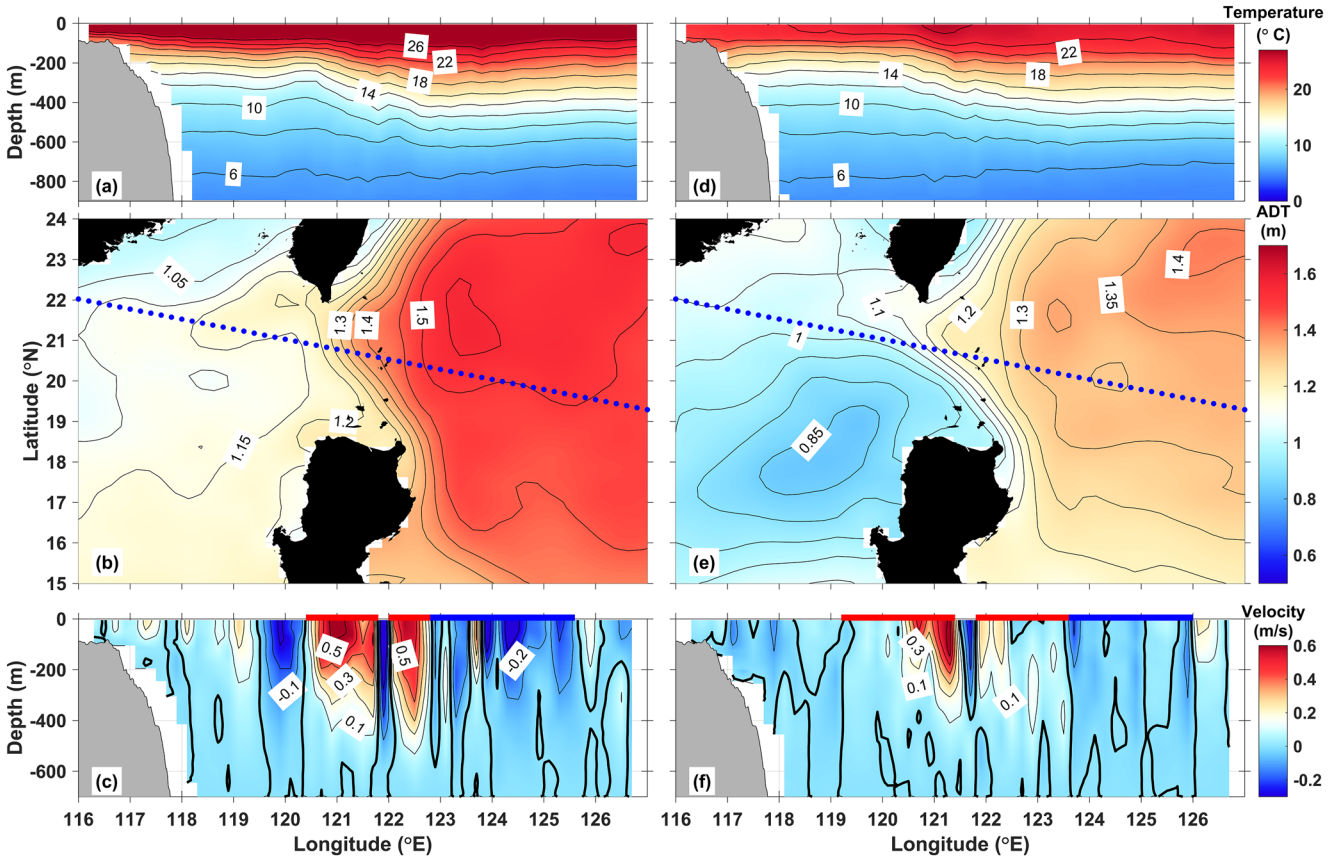

Figure 4. Composite maps. (a) Mean water temperature when the principal component of the first empirical orthogonal function (EOF) mode of water temperature is larger than its standard deviation. (b) Mean absolute dynamic topography when the principal component of the first EOF mode of sea-level anomaly (SLA) is larger than its standard deviation. (c) Mean velocity when the principal component of the first EOF mode of water temperature is larger than its standard deviation. (d–f) are the same as (a–c) but for the period when the principal component of each EOF mode is smaller than minus one standard deviation. The blue dots in (b and e) indicate the XBT stations. The horizontal thick red and blue lines at the upper edge in (c and f) denote the area for calculating the volume transport of Kuroshio's two branches and of the Kuroshio recirculation.

mode of the SLA is larger (smaller) than its positive (negative) standard deviation (Figures 6b and 6e), the Kuroshio recirculation is located to the east of LS (east of Taiwan) and intensifies the Kuroshio northeast of Luzon (east of Taiwan).

The composite map of geostrophic velocity normal to the section shows that the Kuroshio is strong (weak) in the period when the principal component of water temperature is larger (smaller) than the positive

Table 1
Volume Transport (VT), Flow Width (FW, Which is Projected to the Direction Normal to the Current Derived From the Angle Between the Section and the Current, According to Figures 4b and 4e) and the Longitudinal Range (RG) at Section PX44 in the Warm and Cold months

		West branch	East branch	Island wake	Recirculation gyre	Kuroshio region
Warm months	VT (Sv)	20.3 ± 5.6	12.7 ± 10.5	−4.0 ± 13.0	−9.6 ± 11.8	19.4 ± 7.3
	FW (km)	129	65	43	302	539
	RG (°E)	120.4–121.8	122–122.8	121.8–122	122.8–125.6	120.4–125.6
Cold months	VT (Sv)	13.6 ± 7.1	8.3 ± 10.3	−1.4 ± 8.3	−3.6 ± 9.1	17.0 ± 8.3
	FW (km)	236	172	43	238	711
	RG (°E)	119.2–121.4	121.8–123.6	121.4–121.8	123.6–126	119.2–126

Note. Positive values denote a northward current.

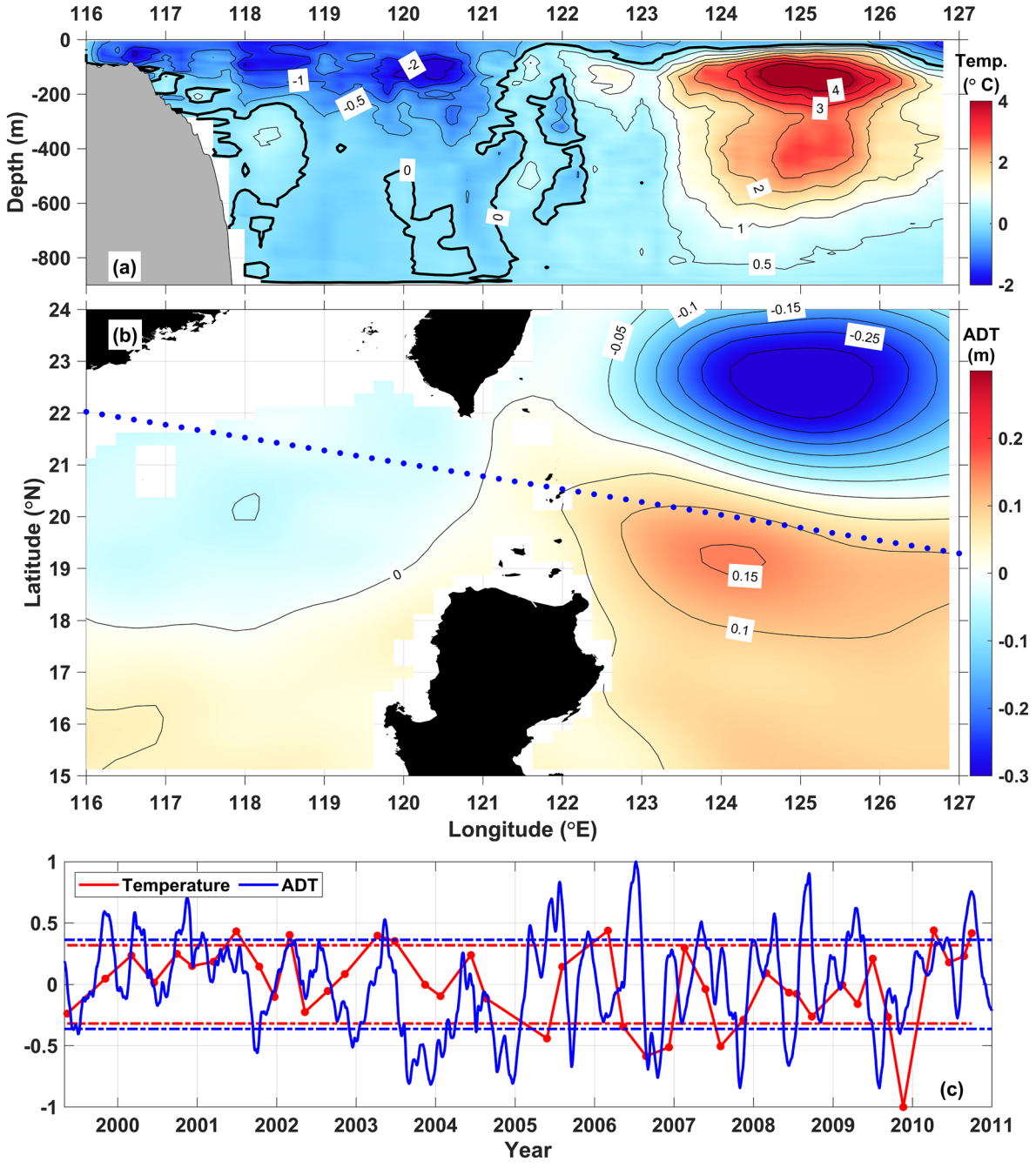

Figure 5. (a) Spatial pattern of the second empirical orthogonal function (EOF) mode of temperature (contour interval: 0.5°C, the thick black line represents 0°C). (b) Spatial pattern of the second EOF mode of sea-level anomaly (SLA) (contour interval: 0.1 m). Blue dots represent the PX44 line. (c) The principal components of the second modes of water temperature (red line) and SLA (blue line). The dashed line represents positive and negative standard deviations.

(negative) standard deviation (Figures 6c and 6f). The volume transport (Table 2) exhibits the same variation except that the Kuroshio recirculation shows an opposite variation to the two Kuroshio branches. This is likely caused by the differences in Kuroshio recirculation and its intersection with the PX44 line during the periods corresponding to the two composite maps; that is, when the Kuroshio recirculation moves southward (northward) and the PX44 line passes through its center (edge), the intersection areas of both positive and negative velocities are large (small), and the volume transport at the section becomes larger (smaller).

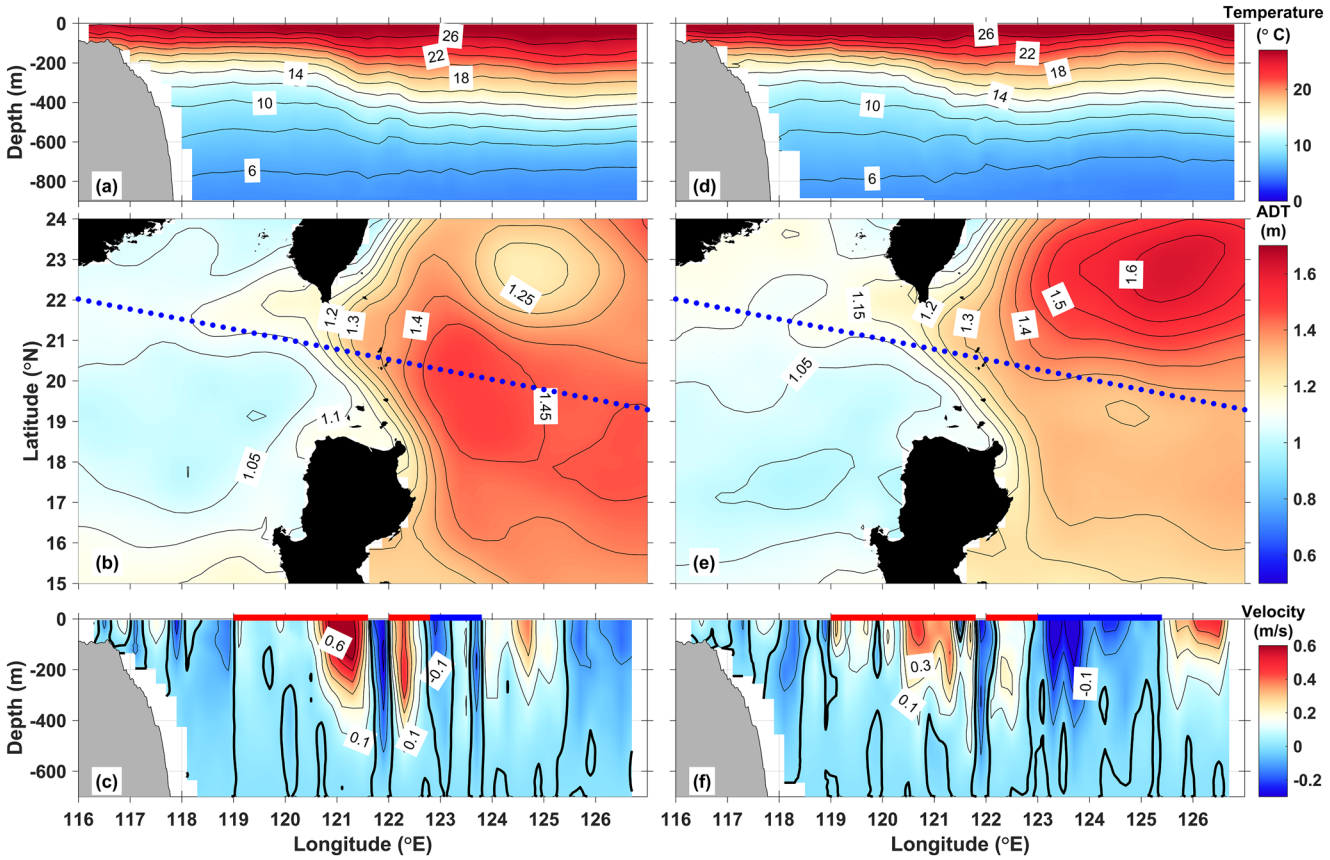

Figure 6. Composite maps, the same as Figure 4 but for their second empirical orthogonal function (EOF) mode.

4. Discussion

4.1. Definition of the Kuroshio and Uncertainties in the Volume Transport

To guarantee the continuity of the Kuroshio volume transport from east of Luzon to the LS and from LS to the east of Taiwan, it is necessary to discuss the definition of the Kuroshio. Andres et al. (2017) demonstrated that the northward increase in the net volume transport (~6 Sv) of the Kuroshio in the upper 1000 m from east of Luzon (14 Sv) to the east of Taiwan (21 Sv) is consistent with the value given by Sverdrup transport theory (~8 Sv east of Luzon and ~14 Sv east of Taiwan). The Kuroshio volume transport in the LS estimated in this study is 18.7 Sv, which is within the range of the above two volume transports given by Andres et al. (2017) for east of Luzon and east of Taiwan.

Table 2
Volume Transport (VT), Flow Width (FW, Which is Projected to the Direction Normal to the Current Derived From the Angle Between the Section and Current, According to Figures 6b and 6e) and the Longitudinal Range (RG) at Section PX44 in the Warm and Cold months

		West branch	East branch	Island wake	Recirculation gyre	Kuroshio region
Positive standard deviation	VT (Sv)	18.6 ± 4.5	8.0 ± 6.8	−3.1 ± 8.4	−1.8 ± 10.5	21.8 ± 5.9
	FW (km)	258	65	65	432	819
	RG (°E)	119–121.6	122–122.8	121.6–122	122.8–123.8	119–123.8
Negative standard deviation	VT (Sv)	18.4 ± 9.4	3.9 ± 2.4	−2.2 ± 8.0	−11.6 ± 7.8	8.5 ± 7.1
	FW (km)	279	86	43	173	668
	RG (°E)	119–121.8	122–123	121.8–122	123–125.4	119–125.4

Note. Positive values denote a northward current.

However, the volume transport of the Kuroshio is sensitive to the choice of the level of no motion. Although a 700 m depth is the historical choice (Gilson & Roemmich, 2002) and has been validated, a thorough investigation is still needed. In the real ocean, the velocity at the level of no motion is not zero. While the flow structure changes little if this velocity is added to the entire water column, volume transport may not. This could be the largest uncertainty in the estimation of the volume transport. Hence, it is essential to examine the extent to which this uncertainty affects the net volume transport of the Kuroshio in the LS.

Some long-term mooring array observations provide information on the mean velocity of the entire water column. Z. Zhang et al. (2015) showed that the mean velocities at 700 m at their LS2 (121°13.78'E 20°42.46'N) and LS3 (121°11.65'E 20°22.16'N) mooring stations were ~0.02 and 0.04 m/s, respectively (Figure 5 in their study; these two sites are near the PX44 section). Considering the orientation of the PX44 section, their normal components to the section do not exceed 0.02 m/s. It is also confirmed that the velocity normal to the section in the depth range of 500–700 m does not exceed 0.02 m/s. On the other hand, the horizontal change in the isotherm (Figures 1d, 4a, 4d, 6a, and 6d) is the smallest at a 700 m depth. Hence, considering the mean state and composite maps, a 700 m depth is a proper choice for the reference level at the PX44 section. For this choice, the uncertainty in the volume transport of the west branch is 0.02 m/s × 900 m × 200 km = 3.6 Sv and that of the east branch is 0.02 m/s × 900 m × 100 km = 1.8 Sv. Since both of them are smaller than their standard deviation, the variations explained by EOF analysis are robust signals.

4.2. Seasonal Variation of the Kuroshio Volume Transport From Upstream to Downstream Regions

In this study, seasonal variations of the Kuroshio at the PX44 line were examined by analyzing the first EOF mode of the SLA and sectional water temperature. Here, we extend this examination by comparing our results with seasonal variations in the upstream Kuroshio east of Luzon, the downstream Kuroshio east of Taiwan, and the Kuroshio-SCS water exchange.

From a climatological view, the volume transport of the Kuroshio east of Taiwan reaches its maximum in July (25.6 Sv) and minimum in April (17.2 Sv, 0–800 m, Gilson & Roemmich, 2002), whereas that east of Luzon is maximal (~32 Sv) in March–April and minimal (~23 Sv) in October–November (entire water column, Yaremchuk & Qu, 2004). To understand the seasonal variations in the volume transport of the Kuroshio from east of Luzon to the east of Taiwan, we examined the surface velocity derived from the Argos drifter data (Figure 7). As drifter data reflect the current at a depth of 15 m, the Ekman component is less than 10 cm/s (Centurioni et al., 2004). The surface velocity from drifters is generally consistent with the composite maps of geostrophic current (Figures 4b and 4e) but reveals some additional detailed features.

In warm months (Figure 7a), the Kuroshio recirculation gyre is located slightly south, intersects more with the PX44 line, and thus has a larger northward and southward volume transport normal to the PX44 line than those in cold months (Table 1). In addition, there is a northward current near northwestern Luzon in warm months (Figure 7a), which was also reported by a model study (Shaw & Chao, 1994) and *in situ* observations from a single cruise (Q. Yang et al., 2010). Before passing through the PX44 line, it enters the Kuroshio (Figure 7a). The trajectory of the drifters that entered the LS also confirmed this northward flow (Figure 7b).

In cold months (Figure 7c), the Kuroshio recirculation gyre is located slightly north and has little intersection with the PX44 line. Part of the Kuroshio flows westward before passing through the PX44 line and is known as the Kuroshio intrusion into the SCS.

Therefore, the Kuroshio intrusion into the SCS and the northerly location of the Kuroshio recirculation in cold months and the northward current from the northwest of Luzon into the Kuroshio and the southerly location of the Kuroshio recirculation in warm months qualitatively explain the seasonal variation in the volume transport normal to the PX44 line.

Because the volume transport of the northward current from the SCS into the Kuroshio in the LS and east of Taiwan in warm months has not been reported in terms of the mean state, we analyze the water properties to provide a general estimation of its contribution. The water temperature and salinity profiles observed by the Argo floats in the region east of Taiwan and east of Luzon and in the SCS (Figure 8) were used to

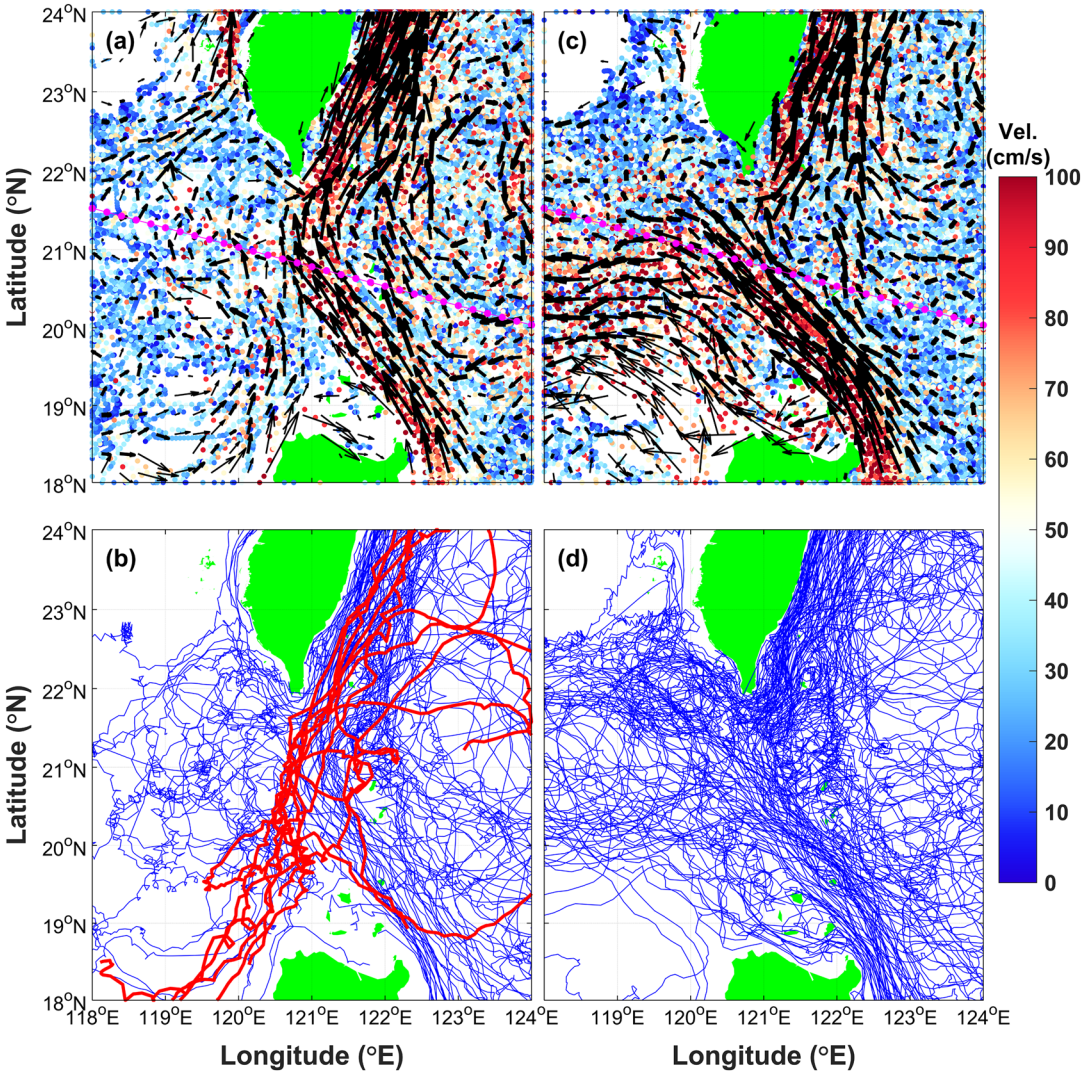

Figure 7. Mean velocity (arrows) derived from the trajectory data of the Argos drifter in a grid with a bin size of 0.25 × 0.25° in (a) warm months (July, August, and September) and (c) cold months (January, February, and March). Colored scatter denotes the magnitude of velocity. The width of the arrows increases with the data number in each grid that was classified as <10, 10–40 and >40. The magenta line denotes the PX44 section. (b and d) Trajectory of the Argos drifter that passed through the Luzon Strait (LS, 120°–122°E, 18°–23°N) in (b) warm months and (d) cold months. The red line in (b) denotes the trajectory of Argos drifters that originated in the South China Sea (SCS) and entered the Kuroshio in the LS and east of Taiwan.

calculate the potential spicity. The potential spicity-potential density relation shows that in warm months, the potential spicity of the Kuroshio east of Taiwan (blue line in Figure 8b) is away from that east of Luzon (red line in Figure 8b) compared with those in cold months (Figure 8e).

Assuming that the seawater of the Kuroshio east of Luzon and the SCS are the two end members, the mixing ratio of the SCS water to the Kuroshio east of Taiwan is 20% in the cold months and 30% in the warm months within the layer lighter than 25.1δ_θ (additional details for this estimation can be found in the supplemental information). This implies that the portion of the upstream Kuroshio water in the Kuroshio east of Taiwan is 10% larger in warm months than in cold months. If we consider the conditions in the cold months as a reference level of water mixing (the flow pattern shows that the Kuroshio directly intrudes the SCS in the cold months), the volume transport of the SCS water in the Kuroshio east of Taiwan should be ~1.3 Sv, which is 10% of the net volume transport (12.8 Sv) within layers lighter than 25.1δ_θ in the Kuroshio region.

Hence, to what extent the Kuroshio-SCS water exchange contributes to the difference of the Kuroshio volume transport east of Luzon and in the LS can be considered. We obtain 18.1 Sv (19.4–1.3 Sv) by subtracting

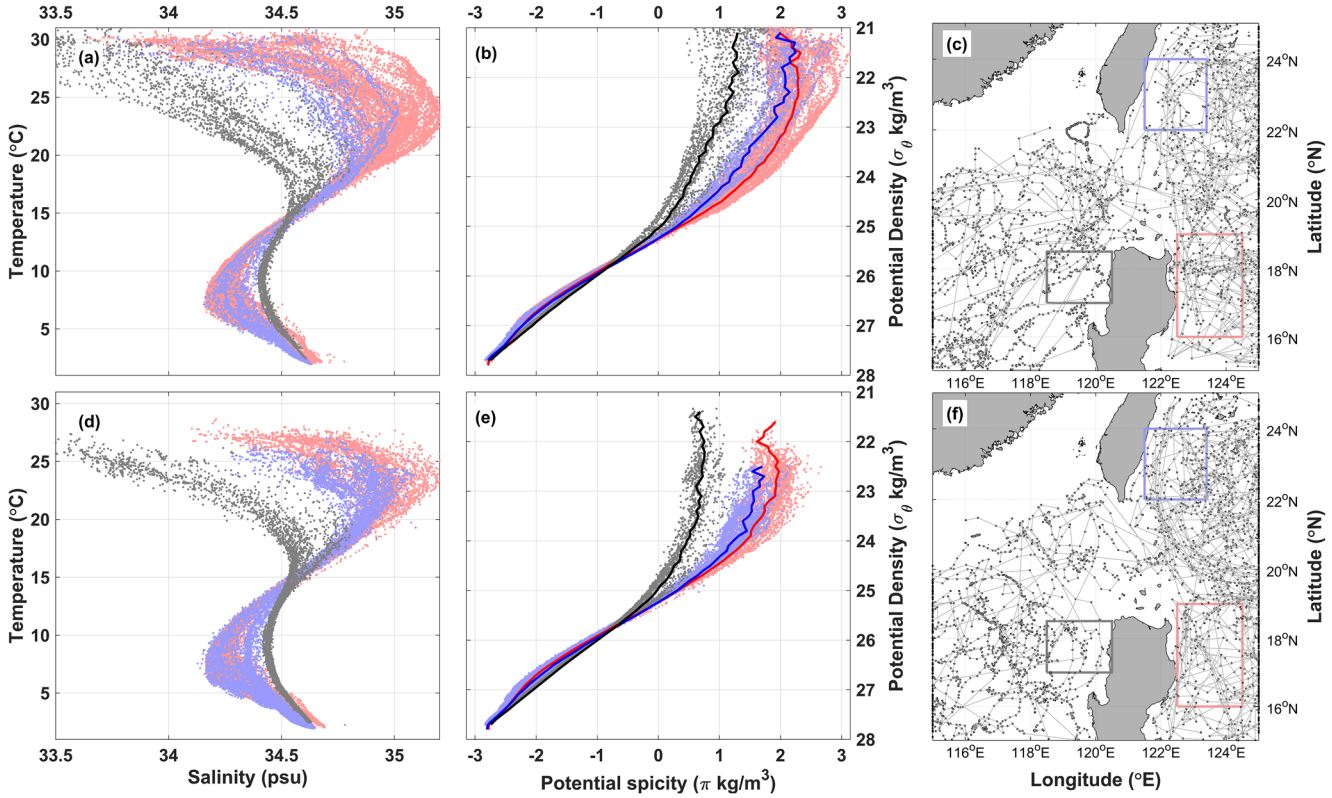

Figure 8. (a and d) Temperature-salinity relationships; (b and e) potential spicity-potential density relationships. The thin line represents the mean potential spicity; (c and f) spatial distribution of Argo profiles (black dot) and its trajectory (gray line). Blue/red/black dots in (a, d) and (b, e) and blue/red/black lines in (b and e) correspond to the profiles within the blue/red/black rectangle in (c). (a–c) are for the warm months. (d–f) are for the cold months.

the SCS outflow in the warm months, and 20–23.5 Sv (17 Sv + 3–6.5 Sv) by adding the volume transport of the Kuroshio intrusion into the SCS in the cold months. With this exclusion of the impacts of Kuroshio-SCS water exchange, the resultant seasonal variation of the Kuroshio transport east of Taiwan is consistent with that east of Luzon.

On the other hand, the mesoscale eddy is reported to have seasonality in this region (Chang & Oey, 2011) because of the instability of the Subtropical Counter Current - North Equatorial Current system (STCC-NEC). Qiu et al. (2014) suggested that the eddy kinetic energy within the STCC band (18°–28°N and 135°–160°E) reaches a maximum in May and April. Considering the necessary time of mesoscale eddies propagating from the STCC band to LS (8.4 months, calculated by the distance between 120° and 135°E and the mean propagating speed of 7.2 cm/s, G. Yang et al., 2013), the eddies within the STCC band in May will impact the Kuroshio in the LS in the cold months. G. Yang et al. (2013) demonstrated that the latitudinal band of the LS is dominated by cyclonic eddies, which tend to decrease Kuroshio volume transport as it approaches the Kuroshio. Hence, mesoscale eddies could be responsible for the decrease in Kuroshio volume transport in the LS in cold months. Second, the wind work is also reported to impact the Kuroshio path in the LS. Recently, Z. Sun et al. (2020) demonstrated that the local wind contributes 66% to the Kuroshio loop current (the transition state between the leaping path and leaking path when the mesoscale eddies interact with the Kuroshio). However, how the local wind affects the preference of the Kuroshio path in the LS is not quantitatively discussed. Hence, it is necessary to quantify their contribution in the future.

The Kuroshio favors the leaping (leaking) path in the warm (cold) months when the Kuroshio volume transport is small (large) east of Luzon but large (small) in the LS. These results imply that the "teapot effect" (Sheremet, 2001, when the upstream volume transport of a western boundary current increased, it tends to leap over the gap, and vice versa) cannot explain the seasonal variation of the Kuroshio in the LS. Hence, the mesoscale eddy and local wind work should be considered.

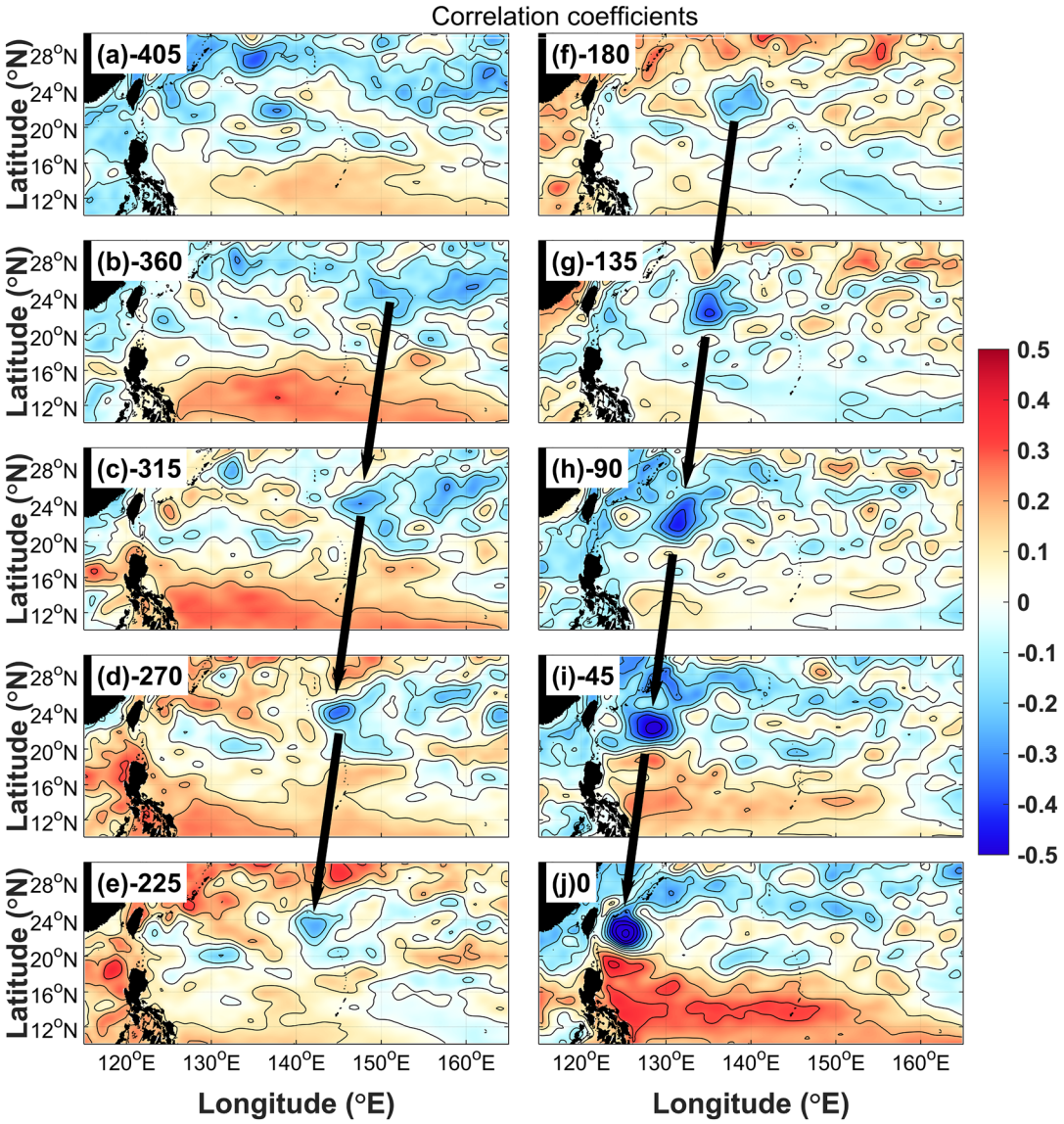

Figure 9. Lag correlation coefficients. (a–i) SLA leads the second empirical orthogonal function (EOF) mode of sea-level anomaly (SLA) by 405, 360, ..., 45, and 0 days. The time interval between two neighboring panels is 45 days.

4.3. Cause of the Second EOF Mode

To determine the cause of the second EOF mode, we calculated the lag correlation coefficient between the principal component of the second EOF mode of the SLA and the SLA over an area extending to 170°E (Figure 9). It is likely that the SLA propagating at the latitude band (21°–25°N) where Taiwan is located (Figure 9b), rather than that at the latitude band (18°–21°N) where the LS is located, is responsible for the second EOF mode of the SLA. The SLA is first recognized at ~150°E (Figures 9b and 9c) and propagates westward to ~130°E (Figures 9h and 9i), where another SLA with an opposite sign appears to its south. The two SLAs then continue their westward propagation and increase their intensity. Once they reach the areas east of Taiwan and east of LS (Figure 9j), the southern one combines with the local recirculation gyre east of the LS and therefore affects its strength. A positive correlation indicates that an anticyclonic eddy intensifies the recirculation gyre east of the LS and that a cyclonic eddy weakens it. The origin of the SLA at ~150°E is located at the Subtropical Counter Current eddy zone (18°–25°N, 135°–170°E), where intense eddy activity is caused by variations in the baroclinic instability growth rate under different wind stress curl conditions (Qiu & Chen, 2010).

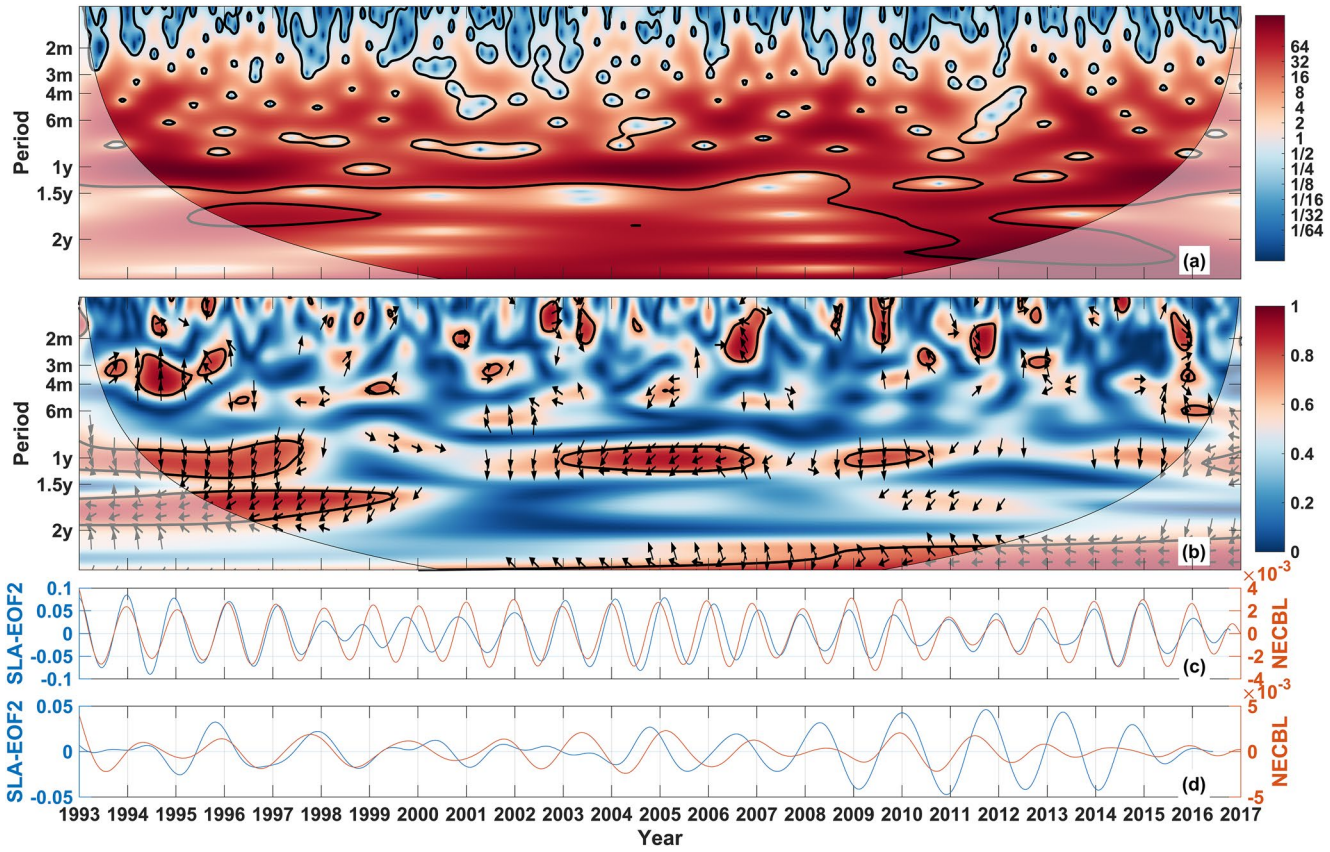

Figure 10. (a) Wavelet power (color shading) of the second empirical orthogonal function (EOF) mode of sea-level anomaly (SLA) during 1993–2017. (b) Wavelet coherence (color shading) between latitudes of the North Equatorial Current Bifurcation (obtained from the SLA in the region of 12°–14°N, 127°–130°E, calculated by $Yp(t) = 11.9 - 0.13 \times SLA(t)$ following Qiu and Chen (2010)) and the second EOF mode of SLA during 1993–2017. The downward arrow indicates that the NECB leads the second EOF mode of SLA by 90° in phase. Leftward arrow indicates antiphase. The 5% significance level against red noise is shown as a thick contour, and the cone of influence (COI) where edge effects might distort the picture is shown as a lighter shade in (a) and (b). (c and d) are the bandpass filtered SLA-EOF2 and NECBL. (c) shows the 1-year variation, and SLA-EOF2 is shifted to the left by a duration of 110 days; (d) shows the 1.5–2-year variation, and SLA-EOF2 is shifted to the left by a duration of 240 days.

Kim and Yin (2004) showed that the North Equatorial Current bifurcation latitude (NECBL) influences the Kuroshio volume transport east of Luzon, and Qu et al. (2004) showed that it further influences transport through the LS. Hence, the intensification of the positive correlation from 130°E (Figure 9i) to the area east of Luzon (Figure 9j) probably also depends on the variation in the NECBL.

To confirm this hypothesis, we extend the temporal range of SLA data to a period from 1993 to 2017 and applied EOF analysis to obtain more information from its principal component (and to reduce edge effects in the wavelet analysis to the 1999–2010 SLA data) by wavelet analysis. The results of EOF analysis for this longer data set are similar to those presented before for the SLA data from 1999 to 2010 (Figure 2f). Wavelet analysis of the principal component of the second EOF mode of the SLA during 1993–2017 demonstrated a dominant time scale of 2–24 months (Figure 10a).

The cross wavelet to the NECBL (Figure 10b) shows that annual (1995–1998, 2003–2007, and 2009–2010) and biennial (1996–2000) variations in the second EOF mode of SLA are correlated with the variations in the NECBL. These periods are consistent with the wavelet results of NECBL (Figure 8a of Qiu & Chen, 2010), which is driven by the wind stress curl in the area of 12°–14°N and 140°–170°E. The annual (biennial) variation in the NECBL leads the second EOF mode of SLA by 90°–135° (135°) in phase, implying that there is a 3–4.5 (8) month phase difference between the second EOF modes of the SLA and NECBL (Figures 10c and 10d). Using the phase difference as the propagation duration from the area of the NECBL to the LS, that is, from 13°N, 128.5°E to 20°N, 122°E, the phase speed is 9 (4.5 month)–13 (3 month) cm/s. Although this speed is larger than the propagation speed of mesoscale eddies at this latitude, considering that the

background flow is northwestward, it is reasonable to believe that the phase difference (3–4.5 months) is a possible propagation duration.

Chang and Oey (2012) suggested that the Philippines-Taiwan Oscillation (PTO, the difference of areal mean wind stress curl between the Taiwan pole, 22°–27°N, 155°–180°E, and Philippines pole, 8°–13°N, 130°–155°E) plays an important role in the thermocline variation east of Taiwan and east of Philippines. By definition, the variation in the wind stress curl over each pole generates a series of mesoscale eddies through Sverdrup convergence and consequently modulates the Kuroshio intrusion into the SCS and circulation and SLAs in the SCS. However, the maximal correlation coefficient is −0.38, for which the PTO leads SLA-EOF2 by 8 months (figure not shown). Indeed, the eddy activity at the latitudinal band of Taiwan is affected by winds over the Taiwan pole, and the NECBL is affected by winds over the Philippines pole. The time for the mesoscale eddies propagating from their origin to the east of Taiwan (~1 year) and the time for the variation from NECBL to the east of Luzon (3–4.5 months) are different. The phase difference explains the small lag correlation between the PTO and SLA-EOF2. Since the spatial pattern of the second EOF mode of SLA is similar to that of the PTO, this mode can be considered the local ocean response to the PTO.

For our case, a plausible explanation is as follows. When the anticyclonic eddy arrives east of Taiwan (Figures 11a–11e), it strengthens the Kuroshio recirculation gyre east of Taiwan. As the Kuroshio recirculation gyre is driven by the low-potential vorticity water from the low-latitude region, the low-potential vorticity water from the NECBL region is also favorable for the strengthening of the Kuroshio recirculation. When the cyclonic eddy impinges on the Kuroshio east of Taiwan (Figures 11f–11j), the downstream advection of the low-potential vorticity water is blocked, and part of it accumulates and forms a positive SLA east of Luzon. Consequently, a strong Kuroshio recirculation gyre forms there. Therefore, the westward-propagating SLAs at the latitude band (21°–23°N) are the main cause of the second EOF mode of the SLA, and the latitudinal variation of the NECB in the upstream region is also a responsible factor.

5. Summary

High-resolution XBT observations collected quarterly during 1999–2010 and daily satellite altimetry data were examined using EOF analyses to investigate the variations of the Kuroshio in the LS. The first EOF modes of water temperature and SLA correspond to seasonal variations. The net volume transport of the two branches of the Kuroshio and Kuroshio recirculation and that over the entire Kuroshio region (the integration of the two branches, island wake, and Kuroshio recirculation) is maximal in warm months (19.4 ± 7.3 Sv) and minimal in cold months (17.0 ± 8.3 Sv). This variation is in contrast to the Kuroshio east of Luzon but similar to that east of Taiwan. Although the upstream Kuroshio east of Luzon shows different seasonal variations, the outflow from the SCS (~1.3 Sv in the layer lighter than $25.1\delta_\theta$) to the Kuroshio in the LS contributes to the seasonal maximum in the Kuroshio volume transport in the warm months, and the Kuroshio intrusion into the SCS in the southern area of the LS contributes to the seasonal minimum in the cold months.

The second EOF modes represent the latitudinal movement of the Kuroshio recirculation. This mode is directly modulated by the westward-propagating SLAs at the latitude band of Taiwan, and the variation in NECBL acts as a secondary factor. The anticyclonic (cyclonic) eddy impinging on the Kuroshio east of Taiwan results in the strengthening (weakening) of the Kuroshio and Kuroshio recirculation. For the strengthening case east of Taiwan, the advection of low-potential vorticity water from the North Equatorial Current bifurcation region also positively contributes, while for the weakening case, the low-PV water accumulates to the east of LS, and thus, the Kuroshio recirculation there is enhanced. In addition, the wavelet analysis suggested that this mode is also probably modulated by low-frequency variations from the NECBL.

Although the XBT and SLA data were used to show dominant variations in the LS, the data have limitations in showing the time series of the Kuroshio volume transport. We examined four-dimensional variational ocean reanalysis (FORA) data (Usui et al., 2017) and found offshore (eastward) movement of the Kuroshio during February 2004 September 2004 and November 2009 (more details are provided in the supporting information). Since the conclusions of this study are through analyzing observations, future studies based on FORA output are expected.

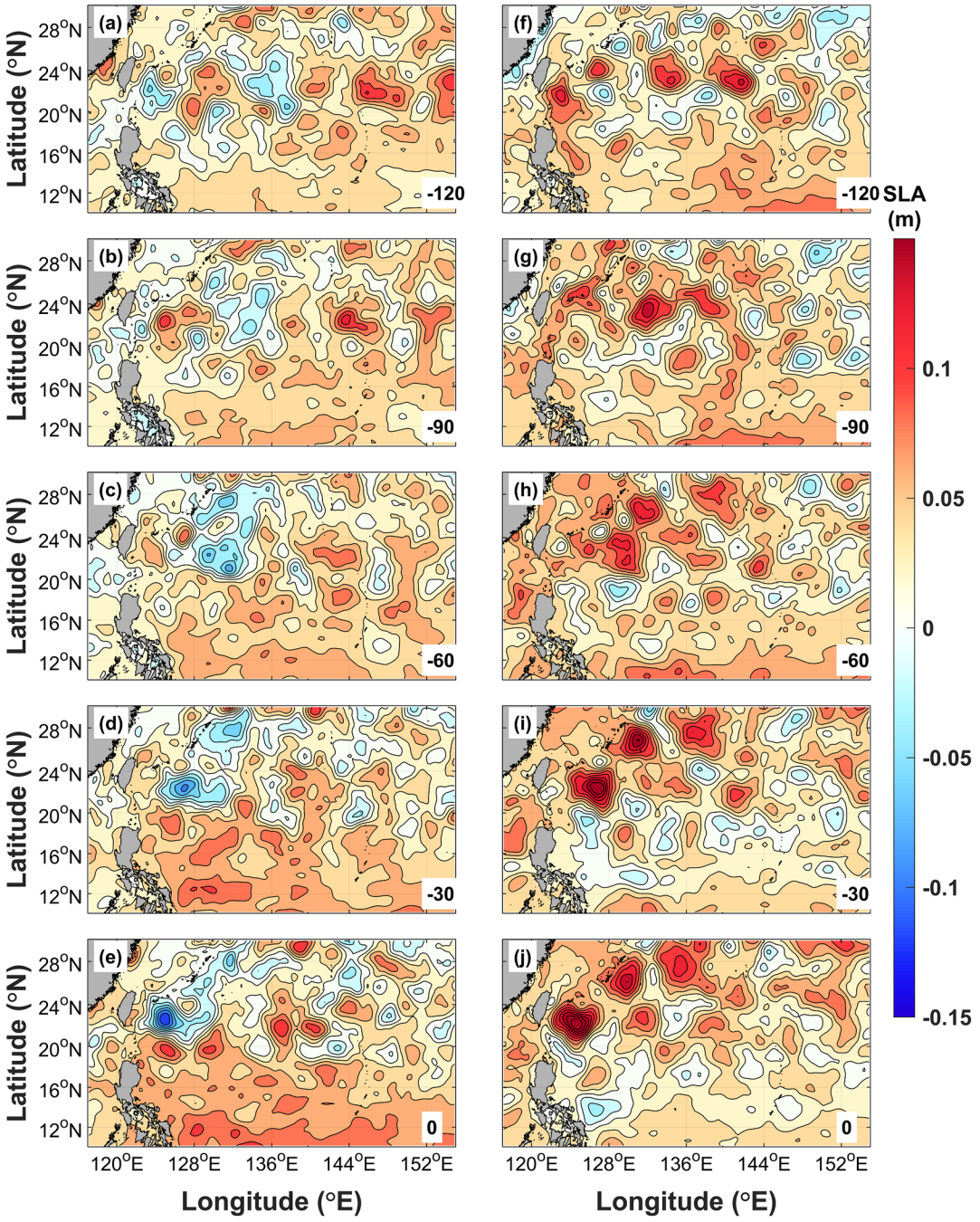

Figure 11. Lag composites of positive (left panels, a–e) and negative (right panels, f–j) events. For any two adjacent panels, the upper panel leads the lower by 30 days. The bottom one is the composite without a time lag.

Data Availability Statement

The data used in this study are available from the Scripps High Resolution XBT program (www-hrx.ucsd.edu), AVISO (http://marine.copernicus.eu), JAMSTEC (http://www.jamstec.go.jp/ARGO/argo_web/argo/?page_id=83&lang=en), NOAA (https://www.aoml.noaa.gov/phod/gdp/index.php) and FORA (http://synthesis.jamstec.go.jp/FORA/).

Acknowledgments
This study was supported by the National Natural Science Foundation of China (grant numbers 41920104006 and 41776107); China Postdoctoral Science Foundation (grant 2020M681969); Scientific Research Fund of SIO, MNR (JZ2001, JB2105); Project of State Key Laboratory of Satellite Ocean Environment Dynamics, SIO (SOEDZZ2106); and grants from the Ministry of Education, Culture, Sports, Science and Technology, Japan (MEXT) to the project on Joint Usage/Research Center—Leading Academia in Marine and Environmental Research (LaMer). X. Guo thanks support by JSPS KAKENHI grant number (17H02959). The authors appreciate three anonymous reviewers for their helpful comments and Dr. L. Oey for his suggestion on revision. Y. Long thanks Dr R.B. Ding for his suggestions in the revision work.

References

Andres, M., Mensah, V., Jan, S., Chang, M.-H., Yang, Y.-J., Lee, C. M., et al. (2017). Downstream evolution of the Kuroshio's time-varying transport and velocity structure. *Journal of Geophysical Research: Oceans*, *122*, 3519–3542. https://doi.org/10.1002/2016JC012519

Atkinson, L. P. (2010). Western Boundary Currents. In K. K. Liu, L. Atkinson, R. Quiñones, & L. Talaue-McManus. (Eds.), *Carbon and nutrient fluxes in continental margins. Global change—The IGBP series* (pp. 121–169). Berlin, Heidelberg: Springer. https://doi.org/10.1007/978-3-540-92735-8_3

Centurioni, L., Niiler, P. P., & Lee, D. (2004). Observations of inflow of Philippine Sea surface water into the South China Sea through the Luzon Strait. *Journal of Physical Oceanography*, *34*(1), 113–121. https://doi.org/10.1175/1520-0485(2004)034<0113:OOIOPS>2.0.CO;2

Chang, Y.-L., & Oey, L.-Y. (2011). Interannual and seasonal variations of Kuroshio transport east of Taiwan inferred from 29 Years of Tide-Gauge Data. *Geophysical Research Letters*, *38*(8), L08603. https://doi.org/10.1029/2011GL047062

Chang, Y.-L., & Oey, L.-Y. (2012). The Philippines-Taiwan Oscillation: Monsoon-like interannual oscillation of the subtropical-tropical western North Pacific wind system and its impact on the ocean. *Journal of Climate*, *25*(5), 1597–1618. https://doi.org/10.1175/JCLI-D-11-00158.1

Farris, A., & Wimbush, M. (1996). Wind-induced Kuroshio intrusion into the South China Sea. *Journal of Oceanography*, *52*, 771–784. https://doi.org/10.1007/BF02239465

Gilson, J., & Roemmich, D. (2002). Mean and temporal variability in Kuroshio geostrophic transport south of Taiwan (1993–2001). *Journal of Oceanography*, *58*, 183–195. https://doi.org/10.1023/A:1015841120927

Hosoda, S., Ohira, T., & Nakamura, T. (2008). A monthly mean dataset of global oceanic temperature and salinity derived from Argo float observations. *JAMSTEC Report of Research and Development*, *8*, 47–59. https://doi.org/10.5918/jamstecr.8.47

Hu, J., Kawamura, H., Hongi, H., & Qi, Y. (2000). A review on the currents in the South China Sea: Seasonal circulation, South China Sea Warm Current and Kuroshio intrusion. *Journal of Oceanography*, *56*, 607–624. https://doi.org/10.1023/A:1011117531252

Huang, R. X., Yu, L.-S., & Zhou, S.-Q. (2018). New definition of potential spicity by the least square method. *Journal of Geophysical Research: Oceans*, *123*, 7351–7365. https://doi.org/10.1029/2018JC014306

Huang, Z., Zhuang, W., Hu, J., & Huang, B. (2019). Observations of the Luzon Cold Eddy in the northeastern South China Sea in May 2017. *Journal of Oceanography*, *75*(5), 415–422. https://doi.org/10.1007/s10872-019-00510-z

Jan, S., Yang, Y. J., Wang, J., Mensah, V., Kuo, T.-H., Chiou, M.-D., et al. (2015). Large variability of the Kuroshio at 23.75°N east of Taiwan. *Journal of Geophysical Research: Oceans*, *120*, 1825–1840. https://doi.org/10.1002/2014JC010614

Kim, & Yin, Y. (2004). Seasonal and interannual variations of the north equatorial current bifurcation in a high-resolution OGCM. *Journal of Geophysical Research*, *109*(C3), C03040. https://doi.org/10.1029/2003JC00201310.1029/2003jc002013

Li, L., Nowlin, W. D., Jr, & Su, J. L. (1998). Anticyclonic rings from the Kuroshio in the South China Sea. *Deep-Sea Research Part I*, *45*, 1469–1482. https://doi.org/10.1016/S0967-0637(98)00026-0

Liang, W. D., Yang, Y. J., Tang, T. Y., & Chuang, W. S. (2008). Kuroshio in the Luzon Strait. *Journal of Geophysical Research*, *113*, C08048. https://doi.org/10.1029/2007JC004609

Lien, R.-C., Ma, B., Cheng, Y.-H., Ho, C.-R., Qiu, B., Lee, C. M., & Chang, M.-H. (2014). Modulation of Kuroshio transport by mesoscale eddies at the Luzon Strait entrance. *Journal of Geophysical Research: Oceans*, *119*, 2129–2142. https://doi.org/10.1002/2013JC009548

Lin, Y.-C., Oey, L.-Y., Wang, J., & Liu, K. K. (2016). Rossby waves and eddies observed at a temperature mooring in northern South China Sea. *Journal of Physical Oceanography*, *46*(2), 517–535. https://doi.org/10.1175/JPO-D-15-0094.1

Liu, Q. Y., Arata, K., & Su, J. L. (2008). Recent progress in studies of the South China Sea circulation. *Journal of Oceanography*, *64*, 753–762. https://doi.org/10.1007/s10872-008-0063-8

Nan, F., He, Z., Zhou, H., & Wang, D. (2011). Three long-lived anticyclonic eddies in the Northern South China Sea. *Journal of Geophysical Research*, *116*, C05002. https://doi.org/10.1029/2010JC006790

Nan, F., Xue, H., Chai, F., Shi, L., Shi, M., & Guo, P. (2011). Identification of different types of Kuroshio intrusion into the South China Sea. *Ocean Dynamics*, *61*(9), 1291–1304. https://doi.org/10.1007/s10236-011-0426-3

Nan, F., Xue, H., & Yu, F. (2015). Kuroshio intrusion into the South China Sea: A review. *Progress in Oceanography*, *137*, 314–333. https://doi.org/10.1016/j.pocean.2014.05.012

Qiu, B., & Chen, S. (2010). Interannual-to-decadal variability in the bifurcation of the north equatorial current off the Philippines. *Journal of Physical Oceanography*, *40*(11), 2525–2538. https://doi.org/10.1175/2010JPO4462.1

Qiu, B., Chen, S., Klein, P., Sasaki, H., & Sasai, Y. (2014). Seasonal mesoscale and submesoscale eddy variability along the north Pacific subtropical countercurrent. *Journal of Physical Oceanography*, *44*(12), 3079–3098. https://doi.org/10.1175/JPO-D-14-0071.1

Qu, T., Kim, Y. Y., Yaremchuk, M., Tozuka, T., Ishida, A., & Yamagata, T. (2004). Can the Luzon Strait transport play a role in conveying the impact of ENSO to the South China Sea? *Journal of Climate*, *17*, 3644–3657. https://doi.org/10.1175/1520-0442(2004)0172.0.CO10.1175/1520-0442(2004)017<3644:clstpa>2.0.co;2

Qu, T., Mitsudera, H., & Yamagata, T. (2000). Intrusion of the North Pacific waters into the South China Sea. *Journal of Geophysical Research*, *105*, 6415–6424. https://doi.org/10.1029/1999JC900323

Shaw, P.-T. (1991). The seasonal variation of the intrusion of the Philippine Sea Water into the South China Sea. *Journal of Geophysical Research*, *96*(C1), 821–827. https://doi.org/10.1029/90JC02367

Shaw, P. T., & Chao, S. Y. (1994). Surface circulation in the South China Sea. *Deep-Sea Research*, *41*(11–12), 1663–1683. https://doi.org/10.1016/0967-0637(94)90067-1

Sheremet, V. A. (2001). Hysteresis of a Western Boundary Current Leaping across a Gap. *Journal of Physical Oceanography*, *31*, 1247–1259. https://doi.org/10.1175/1520-0485(2001)031<1247:HOAWBC>2.0.CO;2

Sheu, W. J., Wu, C. R., & Oey, L. (2010). Blocking and westward passage of eddies in the Luzon Strait. *Deep-sea Research Part II-topical Studies in Oceanography*, *57*(19), 1783–1791. https://doi.org/10.1016/j.dsr2.2010.04.004

Sprintall, J., & Roemmich, D. (1999). Characterizing the structure of the surface layer in the Pacific Ocean. *Journal of Geophysical Research*, *104*, 23297–23311. https://doi.org/10.1029/1999JC900179

Sun, R., Wang, G., & Chen, C. (2016). The Kuroshio bifurcation associated with islands at the Luzon Strait. *Geophysical Research Letters*, *43*, 5768–5774. https://doi.org/10.1002/2016GL069652

Sun, Z., Zhang, Z., Qiu, B., Zhang, X., Zhou, C., Huang, X., et al. (2020). Three-Dimensional structure and interannual variability of the Kuroshio loop current in the northeastern South China Sea. *Journal of Physical Oceanography*, *50*, 2437–2455. https://doi.org/10.1175/jpo-d-20-0058.1

Usui, N., Wakamatsu, T., Tanaka, Y., Hirose, N., Toyoda, T., Nishikawa, S., et al. (2017). Four-dimensional variational ocean reanalysis: A 30-year high-resolution dataset in the western north pacific (FORA-WNP30). *Journal of Oceanography*, *73*(2), 205–233. https://doi.org/10.1007/s10872-016-0398-5

Wang, Q., Zeng, L., Chen, J., He, Y., Zhou, W., & Wang, D. (2020). The linkage of Kuroshio intrusion and mesoscale eddy variability in the northern South China Sea: Subsurface speed maximum. *Geophysical Research Letters*, *47*(11), e2020GL087034. https://doi.org/10.1029/2020GL08703410.1029/2020gl087034

Wang, Q., Zeng, L., Shu, Y., Liu, Q., & Wang, D. (2019). Interannual variability of South China Sea winter circulation: Response to Luzon strait transport and El Nino wind. *Climate Dynamics*, *54*(1/2), 1145–1159. https://doi.org/10.1007/s00382-019-05050-210.1007/s00382-019-05050-2

Wu, C.-R., & Hsin, Y.-C. (2012). The forcing mechanism leading to the Kuroshio intrusion into the South China Sea. *Journal of Geophysical Research*, *117*, C07015. https://doi.org/10.1029/2012jc007968

Xu, F.-H., & Oey, L.-Y. (2014). State analysis using the local ensemble transform Kalman filter (LETKF) and the three-layer circulation structure of the Luzon Strait and the South China Sea. *Ocean Dynamics*, *64*(6), 905–923. https://doi.org/10.1007/s10236-014-0720-y

Xu, F.-H., & Oey, L.-Y., (2015). Seasonal SSH Variability of the Northern South China Sea. *Journal of Physical Oceanography*, *45*(6), 1595–1609. https://doi.org/10.1175/JPO-D-14-0193.1

Yan, X., Zhu, X.-H., Pang, C., & Zhang, L. (2016). Effects of mesoscale eddies on the volume transport and branch pattern of the Kuroshio east of Taiwan. *Journal of Geophysical Research: Oceans*, *121*, 7683–7700. https://doi.org/10.1002/2016JC01203810.1002/2016jc012038

Yang, G., Wang, F., Li, Y., & Lin, P. (2013). Mesoscale eddies in the northwestern subtropical Pacific Ocean: Statistical characteristics and three-dimensional structures. *Journal of Geophysical Research: Oceans*, *118*, 1906–1925. https://doi.org/10.1002/jgrc.20164

Yang, Q., Tian, J., & Zhao, W. (2010). Observation of Luzon strait transport in summer 2007. *Deep Sea Research Part I: Oceanographic Research Papers*, *57*, 670–676. https://doi.org/10.1016/j.dsr.2010.02.004

Yaremchuk, M., & Qu, T. (2004). Seasonal variability of the large-scale currents near the coast of the Philippines. *Journal of Physical Oceanography*, *34*(4), 844–855. https://doi.org/10.1175/1520-0485(2004)034<0844:svotlc>2.0.co;2

Yuan, D., Han, W., & Hu, D. (2006). Surface Kuroshio path in the Luzon Strait area derived from satellite remote sensing data. *Journal of Geophysical Research*, *111*, C11007. https://doi.org/10.1029/2005JC003412

Yuan, D., Song, X., Yang, Y., & Dewar, W. K. (2019). Dynamics of mesoscale eddies interacting with a western boundary current flowing by a gap. *Journal of Geophysical Research: Oceans*, *124*, 4117–4132. https://doi.org/10.1029/2019JC014949

Yuan, Y., Liao, G., Yang, C., Liu, Z., Chen, H., & Wang, Z. (2014). Summer Kuroshio Intrusion through the Luzon Strait confirmed from observations and a diagnostic model in summer 2009. *Progress in Oceanography*, *121*, 44–59. https://doi.org/10.1016/j.pocean.2013.10.003

Zhang, D., Lee, T. N., Johns, W. E., Liu, C., & Zantopp, R. J. (2000). The Kuroshio East of Taiwan: Modes of variability and relationship to Interior ocean mesoscale eddies. *Journal of Physical Oceanography*, *31*(4), 1054–1074. https://doi.org/10.1175/1520-0485(2001)031<1054:TKEOTM>2.0.CO;2

Zhang, Z., Zhao, W., Qiu, B., & Tian, J. (2017). Anticyclonic eddy sheddings from Kuroshio loop and the accompanying cyclonic eddy in the northeastern South China Sea. *Journal of Physical Oceanography*, *47*, 1243–1259. https://doi.org/10.1175/JPO-D-16-0185.1

Zhang, Z., Zhao, W., Tian, J., & Liang, X. (2013). A mesoscale eddy pair southwest of Taiwan and its influence on deep circulation. *Journal of Geophysical Research: Oceans*, *118*, 6479–6494. https://doi.org/10.1002/2013JC008994

Zhang, Z., Zhao, W., Tian, J., Yang, Q., & Qu, T. (2015). Spatial structure and temporal variability of the zonal flow in the Luzon Strait. *Journal of Geophysical Research: Oceans*, *120*, 759–776. https://doi.org/10.1002/2014JC010308

Zheng, Q., Tai, C., Hu, J., Lin, H., Zhang, R., Su, F., & Yang, X. (2011). Satellite altimeter observations of nonlinear Rossby eddy-Kuroshio interaction at the Luzon Strait. *Journal of Oceanography*, *67*(4), 365–376. https://doi.org/10.1007/s10872-011-0035-2